U.S. Department
of Transportation

**Federal Railroad
Administration**

Real-Time Measurement of Track Modulus from a Moving Car

Office of Research and
Development
Washington, DC 20590

DOT/FRA/ORD-05/05

December 2005

REPORT DOCUMENTATION PAGE

FORM APPROVED
OMB NO. 0704-0188

1. AGENCY USE ONLY *(Leave blank)*	2. REPORT DATE	3. REPORT TYPE AND DATES COVERED
	January 2006	Final Report 2005-2006

4. TITLE AND SUBTITLE

Real-Time Measurement of Track Modulus from a Moving Car

5. FUNDING NUMBERS

6. AUTHOR(S)

Shane Farritor

7. PERFORMING ORGANIZATION NAME(S) AND ADDRESS(ES)

8. PERFORMING ORGANIZATION REPORT NUMBERS

DTFR-53-03-G-00006

9. SPONSORING/MONITORING AGENGY NAME(S) AND ADDRESS(ES)

U.S. Department of Transportation
Federal Railroad Administration
Office of Research and Development, MS 20
1120 Vermont Avenue, NW
Washington, DC 20590

10. SPONSORING/MONITORING AGENCY REPORT NUMBER

11. SUPPLEMENTARY NOTES

12a. DISTRIBUTION/AVAILABILITY STATEMENT

This document is available through National Technical Information Service, Springfield, VA 22161.

12b. DISTRIBUTION CODE

13. ABSTRACT

The economic constraints of passenger and freight railroad traffic are moving the industry to higher speed rail vehicles and higher axle loads. The dynamics of high-speed trains and the high static loads produce high stresses in the rail components. Track performance under these conditions is strongly related to the vertical track modulus—the relationship between the rail deflection and the vertical applied load. Both low track modulus and large variations in track modulus increase dynamic loading leading to increased maintenance needs and reduced ride quality. Currently, no widely accepted method to measure vertical track modulus from a rail car traveling at significant train speed exists.

This report presents a method to measure vertical track modulus from a moving rail car. The method measures the shape of the rail deflection under the moving car and uses a mathematical track model to estimate modulus. The report presents theoretical, simulation, and experimental results.

14. SUBJECT TERMS	15. NUMBER OF PAGES
Track modulus, rail car, high-speed trains	37
	16. PRICE CODE

17. SECURITY CLASSIFICATION	18. SECURITY CLASSIFICATION OF THIS PAGE	19. SECURITY CLASSIFICATION OF ABSTRACT	20. LIMITATION OF ABSTRACT
UNCLASSIFIED	UNCLASSIFIED	UNCLASSIFIED	UNLIMITED

NSN 7540-01-280-5500

Standard Form 298 (Rec. 2-89)
Prescribed by ANSI/NISO Std. 239.18
298-102

Table of Contents

List of Figures

ACKNOWLEDGEMENTS

This report presents the results from a 4-year project to develop a system to measure Vertical Track Modulus (VTM) from a moving railcar. The work completed during this project has significantly advanced the state of the art and understanding of VTM data collection and interpretation in the railroad environment. The follow-on phases will implement the techniques presented in this report to create robust automated data collection and interpretation and to further investigate safety-compromising VTM track conditions.

This work was performed at the University of Nebraska-Lincoln under the direction of Dr. Shane Farritor. The authors are grateful to Dwight Clark, Bill GeMeiner, and Mike Boos of the Union Pacific Railroad (UPRR); John Leeper, Mike Oliver, and Hank Lees of the Burlington Northern Santa Fe Railroad (BNSF); and Rich Kotan of Omaha Public Power District (OPPD). These people served on an Industrial Advisory Board that contributed to this research throughout the project.

Mr. Mahmood Fateh of the Federal Railroad Administration (FRA) served as the technical monitor for this project and Dr. Magdy El-Sibaie of FRA contributed to the project. UPRR, BNSF, and OPPD provided access to revenue service track, as well as provided operational support including motive power, train crews, and logistics. UPRR donated a caboose that was refurbished to serve as the crew platform during testing. UPRR also donated a hopper car, and BNSF loaned a tank car to serve as a heavy axle load vehicle for the testing. The authors are also grateful to Dr. Ted Sussmann of the U.S. Department of Transportation Volpe Center for his technical input and guidance, as well as useful comments on the draft versions of this report.

EXECUTIVE SUMMARY

Track quality is a major factor in railroad safety, and one accepted indicator of track quality is the vertical track modulus. Track modulus is defined as the coefficient of proportionality between the vertical rail deflection and the vertical contact pressure between the rail base and track foundation. Railway track has several components that all contribute to track stiffness, including the rail, subgrade, ballast, subballast, ties, and fasteners.

Track modulus is important because it affects track safety, track performance and track maintenance. Both low track modulus and large variations in track modulus are undesirable. Low track modulus has been shown to cause differential settlement that then increases maintenance needs. Large variations in track modulus, such as those often found near bridges and crossings, have been shown to increase dynamic loading. Increased dynamic loading reduces the life of the track components, resulting in shorter maintenance cycles. It has been shown that reducing variations in track modulus at grade (i.e., road) crossings leads to better track performance and less track maintenance. Ride quality, as indicated by vertical acceleration, is also strongly dependent on track modulus.

The economic constraints of passenger and freight rail service are moving the industry to higher speed rail vehicles, and the performance of high-speed trains are strongly dependent on track modulus. It is suggested that track with a high and consistent modulus will allow for higher train speeds and therefore increased performance and revenue.

This research presents the design, analysis, and testing of an on-board, non-contact track modulus measurement system. On-board measurements are difficult because no stable reference frame exists. The system presented here measures vertical rail displacement relative to the wheel/rail contact point, and these relative measurements are combined with an analytical model of the track structure and the measured vehicle loads (weight and dynamic forces) to estimate the modulus.

The sensor system consists of a digital vision system and two line lasers. The camera and line lasers are rigidly attached to a bracket mounted to the sideframe (structural member that connects axles) of a truck (two-axle assembly). These lasers are projected at an acute angle (~30˚). They cross and create curves (because of the curved profile of the rail head) across the surface of the rail. On softer track the rail will rise relative to the wheel/rail contact point, and the laser lines as observed by the camera will move closer together. Conversely, the distance between the lasers will increase on stiffer track. The minimum distance between these lines, d, can be related mathematically to the track modulus. Using line lasers allows the system to compensate for lateral movement of the rail relative to the camera and for changes in rail profile.

This research presents the mathematical models used to estimate track modulus from the laser measurements. The system is evaluated using computer simulations and field testing. Field testing was conducted at several locations on Class III, IV, and V tracks. Independent trackside measurements of rail deflection are used to confirm the on-board measurements.

1 TECHNICAL INVESTIGATION

1.1 Introduction

Track quality is a major factor in railroad safety, and one accepted indicator of track quality is the vertical track modulus. Track modulus is defined as the coefficient of proportionality between the vertical rail deflection and the vertical contact pressure between the rail base and track foundation (Cai, et al., 1994); it can be restated as the supporting force per unit length of rail, per unit rail deflection (Selig and Li, 1994).

Railway track has several components that all contribute to track stiffness, including the rail, subgrade, ballast, subballast, ties, and fasteners. The rail directly supports the train wheels and is supported on a rail pad and held in place with fasteners to crossties. The crossties rest on a layer of rock ballast and subballast used to provide drainage. The soil below the subballast is the subgrade.

The subgrade resilient modulus and subgrade thickness have the strongest influence on track modulus. These parameters depend upon the physical state of the soil, the stress state of the soil, and the soil type (Li and Selig, 1994; Selig and Li, 1994). Track modulus increases with increasing subgrade resilient modulus and decreases with increasing subgrade layer thickness (Selig and Li, 1994). Ballast layer thickness and fastener stiffness are the next most important factors (Selig and Li, 1994; Li and Selig, 1998). Increasing the thickness of the ballast layer and/or increasing fastener stiffness will increase track modulus (Stewart, 1985; Selig and Li, 1994). This effect is caused by the load being spread over a larger area. The system presented in this research measures the net effective track modulus that includes all these factors.

Track modulus is important because it affects track performance and maintenance requirements. Both low track modulus and large variations in track modulus are undesirable. Low track modulus has been shown to cause differential settlement that then increases maintenance needs (Read, et al., 1994; Ebersohn, et al., 1993). Large variations in track modulus, such as those often found near bridges and crossings, have been shown to increase dynamic loading (Zarembski and Palese, 2003; Davis, et al., 2003). Increased dynamic loading reduces the life of the track components, resulting in shorter maintenance cycles (Davis, et al., 2003). It has been shown that reducing variations in track modulus at grade (i.e., road) crossings leads to better track performance and less track maintenance (Zarembski and Palese, 2003). Ride quality, as indicated by vertical acceleration, is also strongly dependent on track modulus.

The economic constraints of passenger and freight rail service are moving the industry to higher speed rail vehicles, and the performance of high-speed trains are strongly dependent on track modulus. It has been shown that at high speeds there will be an increase in track deflection caused by larger dynamic forces (Carr and Greif, 2000; Heelis, et al., 1999). These forces become significant as rail vehicles reach 50 km/hr (30 mph) (Kerr, 1976) and rail deflections increase with higher vehicle speeds up to a critical speed (Heelis, et al., 1999). It is suggested that track with a high and consistent modulus will allow for higher train speeds and therefore increased performance and revenue (Heelis, et al., 1999).

Previous localized field-testing has shown that it is possible to measure areas of low track modulus, variable track modulus, void deflection, variable total deflection, and inconsistent rail deflection (Sussmann, et al., 2001; Ebersohn and Selig, 1994). In the past such systems have been used to identify sections of track with poor performance. These measurements have been useful; however, they are expensive and are only being made over short distances (~tens of meters). The ability to make these measurements continuously over large sections of track is desirable (Ebersohn and Selig, 1994; Read, et al., 1994).

This research presents the design, analysis, and testing of an on-board, non-contact track modulus measurement system. On-board measurements are difficult because no stable reference frame exists. The system presented here measures vertical rail displacement relative to the wheel/rail contact point, and these relative measurements are combined with an analytical model of the track structure and the measured vehicle loads (weight and dynamic forces) to estimate the track modulus.

The sensor system consists of a digital vision system and two line lasers, as seen in Figure 1. The camera and line lasers are rigidly attached to a bracket mounted to the sideframe (structural member that connects axles) of a truck (two-axle assembly). These lasers are projected at an acute angle (~30˚). They cross and create curves (because of the curved profile of the rail head) across the surface of the rail. On softer track the rail will rise relative to the wheel/rail contact point, and the laser lines as observed by the camera will move closer together. Conversely, the distance between the lasers will increase on stiffer track. The minimum distance between these lines, d, can be related mathematically to the track modulus. Using line lasers allows the system to compensate for lateral movement of the rail relative to the camera and for changes in rail profile.

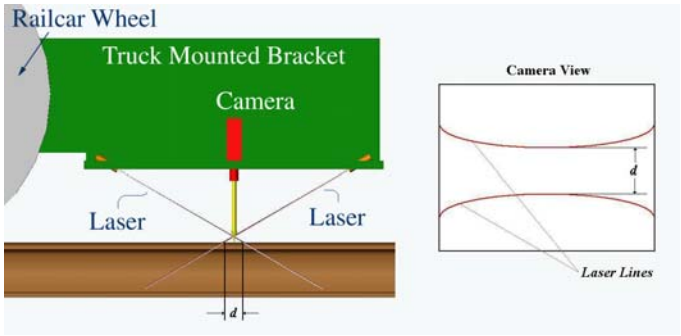

Figure 1. Measurement System

This research presents the mathematical models used to estimate track modulus from the laser measurements. The system is evaluated using computer simulations and field testing. Field testing was conducted at several locations on Class III, IV, and V tracks. Independent trackside measurements of rail deflection are used to confirm the on-board measurements.

1.2 Background and Previous Work

The measurement of vertical track modulus is difficult. Previous measurement systems can be placed in two categories: trackside measurements and onboard measurements. With the trackside approach a section of track is closed to rail traffic, and a work crew uses specialized

equipment to make measurements at various discrete locations. Onboard measurements are made from a moving railcar and are more desirable because they can be made with less interruption of rail traffic and over longer distances. However, current onboard systems are still very labor intensive and move at only slow speeds and are therefore limited to short distances (e.g., hundreds of meters) and still interrupt traffic.

1.2.1 Trackside Measurement of Track Modulus

In all trackside methods rail deflection is measured before and after a static point load is applied. Differences lie in the number of deflection measurements made and how those measurements are used to estimate track modulus. Common trackside approaches include the Beam on Elastic Foundation and the Deflection Basin method.

The Beam on an Elastic Foundation method uses a structural model, known as the Winkler Model, to represent the track system. The Winkler Model represents a point load applied to an infinite Bernoulli beam on an infinite elastic foundation. Trackside measurements of the deflection at the point where the load is applied are taken for a known load and modulus can then be calculated using (Selig and Li, 1994; Cai et al, 1994):

$$u = \frac{1}{4}\left(\frac{1}{EI}\right)^{\frac{1}{3}}\left(\frac{P}{w_0}\right)^{\frac{4}{3}} \tag{1}$$

where:

u is the track modulus.
E is the modulus of elasticity of the rail.
I is the moment of inertia of the rail.
P is the load applied to the track.
w_0 is the deflection of the rail at the loading point.

This method only requires a single measurement, and it has also been suggested to be the best method for field measurement of track modulus (Zarembski and Choros, 1980). Its major limitation is that it provides only information for a single point. In reality, the modulus may be very different only a meter away. In addition, if multiple loads are present (as is the case with multi-axle railway vehicles used to apply the point load), small deflections must be assumed, and superposition is needed. In this case the Winkler Model cannot be simplified as in (1) and an iterative solution is required (Selig and Li, 1994; Cai et al., 1994). Slack in the rail can cause non-linearity in the load/deflection relationship. Therefore, a small load should be applied to determine the zero displacement position for the measurement (Ebersohn and Selig, 1994; Read et al., 1994). A heavy load is then applied and used as the loaded measurement. This further complicates the technique.

The second trackside technique, the Deflection Basin method, uses the vertical equilibrium of the loaded rail to determine track modulus. In this approach rail deflection caused by a point load(s) is measured at several (ideally infinite) locations along the rail and the entire deflected area calculated. Using a force balance this deflected area, or deflection basin, can be shown to be proportional to the integral of the rail deflection (Selig and Li, 1994; Cai et al., 1994):

$$P = \int_{-\infty}^{\infty} q(x)dx = \int_{-\infty}^{\infty} u\delta(x)dx = uA_{\delta} \quad (2)$$

where:

P is the load on the track.
$q(x)$ is the vertical supporting force per unit length.
u is the track modulus.
$\delta(x)$ is the vertical rail deflection.
A_{δ} is the deflection basin area (area between the original and deflected rail positions).
x is the longitudinal distance along the track.

The multiple deflection measurements result here in longer traffic delays (Selig and Li, 1994); heavy and light loads are again used to eliminate slack. Some researchers question the basic assumptions of this method (Kerr and Shenton, 1985).

All the above methods are time consuming and expensive, and all suffer from the major limitation that the measured modulus is only valid along a small length of track.

1.2.2 Onboard Track Modulus Measurement

Previous onboard track modulus measurement systems are similar to systems developed by the military and used in highway research (Carr, 1999). The systems use a long rigid truss that rides on two unloaded wheels. This truss creates a straight line, or cord, that is used as a reference for the measurement. A third wheel is then used to apply a load at midpoint of the cord (or truss), and the relative displacement between the loaded wheel and the unloaded truss is measured. The truss must be long enough, generally 30.48 m (100 ft), so that the two endpoints are not affected by the load at the center of the truss. This method again requires two measurements, one with a light load, made with a similar truss, and the heavy load, to distinguish between changes in geometry and changes in modulus. The output of this approach is a measurement of the relative displacement of the loaded wheel with respect to the unloaded wheel, and track modulus is then estimated.

One vehicle, called the Track Loading Vehicle (TLV), uses this approach (Thompson and Li, 2002). This vehicle is capable of measuring track modulus at speeds of 16.1 km/hr (10 mph). The TLV uses two cars, each with a center load bogie capable of applying loads from 4.45 kN to 267 kN (1 to 60 kips). A light load (13.3 kN or 3 kips) is applied by the first vehicle while a heavier load is applied by the second vehicle. A laser-based system on each vehicle measures the deflections of the rail caused by the center load bogies. The test procedure involves two passes over a section of track, first applying a 44.5 kN (10 kip) load and then a 178 kN (40 kip) load (Thompson and Li, 2002).

The TLV is operational, however, it still has limitations. First, tests are often performed at speeds below 16.1 km/hr (10 mph) so it is difficult to test long section of track (hundreds of miles). Second, significant expense in equipment and personnel are required for operation. For these reasons the TLV has not yet been widely implemented.

This research presents a simple method to determine track modulus from a moving railcar. The sensor system uses a non-contact structured-lighting vision system. The proposed system

is inexpensive and does not require significant support equipment. It has the potential to operate at higher speeds and could potentially be automated. This research presents the theory and design of the system.

1.3 Models of Rail Deflection

The following presents two mathematical planar models of rail deflection. The first is the widely accepted Winkler Model mentioned above, and the second is a new discrete support (crosstie) model used to estimate track modulus in this work. The models are compared, but the field results presented below show the discrete support model is needed when track modulus changes over short distances. Both models assume knowledge of the rail's elastic modulus and cross-sectional geometry which are commonly available for all commercial rail.

1.3.1 The Winkler Model

The Winkler Model describes the deflection of an infinitely long beam resting on an infinite continuous, uniform, elastic foundation in response to a single point load. In this model the deflection of the beam under an applied load is linearly proportional to the pressure between the base of the rail and the foundation. This model has been shown to be an effective method for determining track modulus (Raymond, 1985; Meyer, 2002), and derivations can be found in Kerr, 1976; Boresi and Schmidt, 2003. The vertical deflection of the rail, y, as a function of longitudinal distance along the rail x (referenced from the applied load) is given by:

$$y(x) = -\frac{P\beta}{2u} e^{-\beta \cdot x} \left[\cos(\beta x) + \sin(\beta x)\right] \tag{3}$$

where:

$$\beta = \left(\frac{u}{4EI_z}\right)^{\frac{1}{4}} \tag{4}$$

where:

P is the load on the track.
u is the track modulus.
E is the modulus of elasticity of the rail.
I_z is the moment of inertia of the rail.
x is the longitudinal distance along the rail.

When multiple loads are present, the rail deflections caused by each of the loads are superposed (assuming small vertical deflections) (Boresi and Schmidt, 2003).

Figure 2 shows a plot of the rail deflection given by the Winkler Model over the length of a four-axle coal hopper. The deflection is shown relative to the wheel/rail contact point for five different reasonable values of track modulus (6.89, 13.8, 20.7, 27.6, and 34.5 MPa or 1000, 2000, 3000, 4000, and 5000 lbf/in/in). The model assumes 115 lb rail with an elastic modulus of 206.8 GPa (30,000,000 psi) and an area moment of inertia of 2704 cm^4 (64.97 in^4). Figure 2 shows larger rail displacements with respect to the wheel/rail contact point occur with low track modulus.

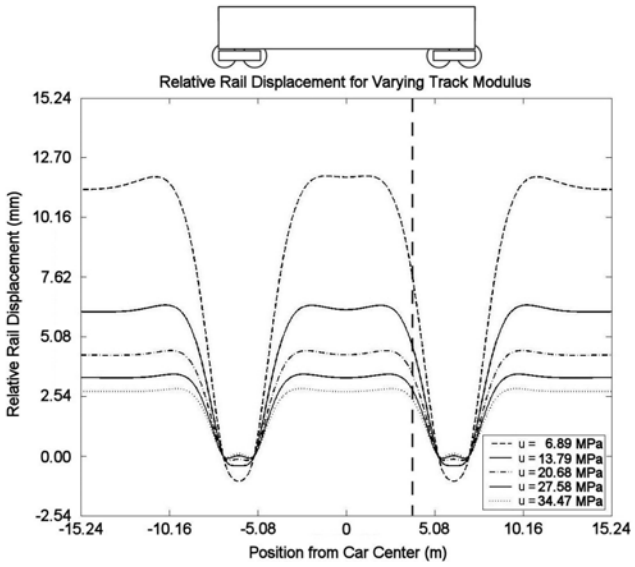

Figure 2. Relative Rail Displacement under a Railcar

Relative to the wheel/rail contact point (as in Figure 2) the rail displacement is most sensitive to track modulus far from the wheel contact point. This variation is used in the measurement system proposed in this research. The sensors that measure track displacement in this work are located approximately 1.25 m (48 in.) toward the center of the car from the third axle (indicated by a dashed line in Figure 2).

1.3.2 Discrete Support Model

The discrete support model describes the rail supported on a number of discrete springs with a single force applied. The discrete springs represent support at the crossties, and the single applied load represents one railcar wheel. At this time, tie support is modeled by linearly elastic springs. This model is more applicable at low speeds, but future work will include viscoelastic behavior. It is expected that measurements of track modulus may vary with train speed because of damping. However, the experimental results in this research suggest rate of deflection may not be significant at speeds below 48 km/hr (30 mph) (Section 1.6.4).

The discrete tie model is shown to be useful in the experimental results (Section 1.6.3) because track modulus can vary from tie to tie. In Figure 3, the proposed model considers only finite lengths of rail and a finite number of ties. To reduce the model's computational requirements (so it can be implemented in real time), the rail is assumed to extend beyond the ties and is fixed at a (large) distance from the last tie. This ensures the boundary conditions are well defined (the rail is flat far away), and the rail shape is continuous.

The deflection in each of the springs (i.e., the rail deflection) can be determined by first solving for the forces in each of the springs using energy methods. The principles of stationary potential energy and Castigliano's theorem on deflections are applied (Boresi and Schmidt, 2003). For these methods to be applicable, small displacements and linear elastic behavior is assumed. The number of equations needed to determine the forces in the springs is equal to the number of springs (i.e., spring forces are the unknowns).

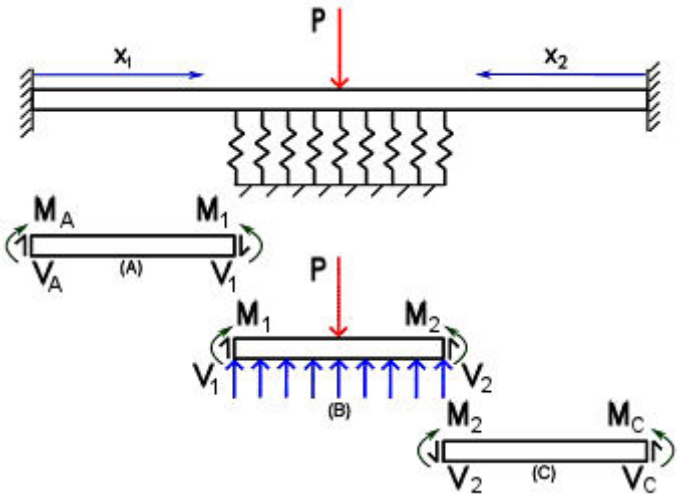

Figure 3. Discrete Model and Free Body Diagram

The discrete support model is similar to the Winkler Model when the ties are uniformly spaced, have uniform stiffness, and the rail is long. Nine ties are used in this work, and experimental trackside measurements have shown this to be sufficient (Norman, 2004).

The moment and shear force in the cantilevered sections of the model (Figure 3(A) and 3(C)) can now be calculated. Static equilibrium requires the moment and shear force for Section A to be:

$$M_1 = M_A + V_A x_1 \tag{5}$$

$$V_1 = V_A \tag{6}$$

Likewise, for Section C:

$$M_2 = M_C + V_C x_2 \tag{7}$$

$$V_2 = V_C \tag{8}$$

The forces in the springs can be determined with energy methods (Figure 3(B)). Section B is split into segments separated by the springs, and the segment's internal moments are found (as in 9 and 11 above) to determine the beam's strain energy from the internal moments, Figure 4. Energy from shear force is small and is neglected (Norman, 2004).

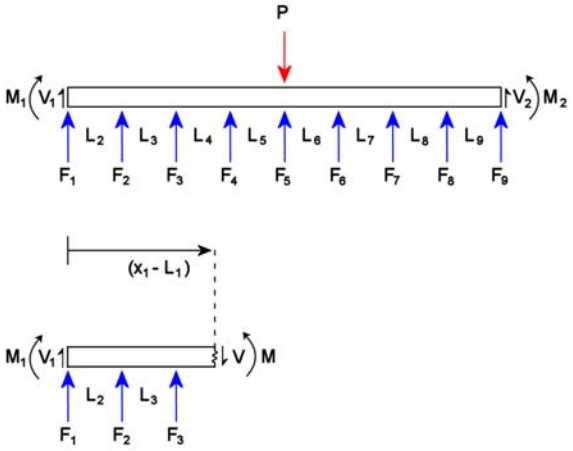

Figure 4. Middle Segment of Discrete Tie Model

The equations for the internal moments in each segment can be written, (13)-(22), where moments M_1 and M_2, and the shear forces V_1 and V_2 are given by equations 9-12. The lengths of each of the segments (i.e., tie spacing) in the beam are given by $L_1 - L_{10}$ and the spring forces are denoted by $F_1 - F_9$ (Figure 4).

$$M = M_1 \quad \text{for } 0 \le x_1 \le L_1 \tag{9}$$

$$M = -\left[M_1 + V_1(x_1 - L_1) + F_1(x_1 - L_1)\right] \quad \text{for } L_1 \le x_1 \le L_1 + L_2 \tag{10}$$

$$M = -\left[M_1 + V_1(x_1 - L_1) + F_1(x_1 - L_1) + F_2(x_1 - L_1 - L_2)\right] \quad \text{for } L_1 + L_2 \le x_1 \le L_1 + L_2 + L_3 \tag{11}$$

$$M = -\begin{bmatrix} M_1 + V_1(x_1 - L_1) + F_1(x_1 - L_1) + F_2(x_1 - L_1 - L_2) \\ + F_3(x_1 - L_1 - L_2 - L_3) \end{bmatrix} \quad \text{for } L_1 + L_2 + L_3 \le x_1 \le L_1 + L_2 + L_3 + L_4 \tag{12}$$

$$M = -\begin{bmatrix} M_1 + V_1(x_1 - L_1) + F_1(x_1 - L_1) + F_2(x_1 - L_1 - L_2) \\ + F_3(x_1 - L_1 - L_2 - L_3) + F_4(x_1 - L_1 - L_2 - L_3 - L_4) \end{bmatrix} \quad \text{for } L_1 + L_2 + L_3 + L_4 \le x_1 \le L_1 + L_2 + L_3 + L_4 + L_5 \tag{13}$$

$$M = \begin{bmatrix} M_2 + V_2(x_2 - L_{10}) + F_9(x_2 - L_{10}) + F_8(x_2 - L_{10} - L_9) \\ + F_7(x_2 - L_{10} - L_9 - L_8) + F_6(x_2 - L_{10} - L_9 - L_8 - L_7) \end{bmatrix} \quad \text{for } L_{10} + L_9 + L_8 + L_7 \le x_2 \le L_{10} + L_9 + L_8 + L_7 + L_6 \tag{14}$$

$$M = \begin{bmatrix} M_2 + V_2(x_2 - L_{10}) + F_9(x_2 - L_{10}) + F_8(x_2 - L_{10} - L_9) \\ + F_7(x_2 - L_{10} - L_9 - L_8) \end{bmatrix} \quad \text{for } L_{10} + L_9 + L_8 \le x_2 \le L_{10} + L_9 + L_8 + L_7 \tag{15}$$

$$M = \left[M_2 + V_2\left(x_2 - L_{10}\right) + F_9\left(x_2 - L_{10}\right) + F_8\left(x_2 - L_{10} - L_9\right)\right]$$
$$\text{for } L_{10} + L_9 \le x_2 \le L_{10} + L_9 + L_8 \tag{16}$$

$$M = \left[M_2 + V_2\left(x_2 - L_{10}\right) + F_9\left(x_2 - L_{10}\right)\right]$$
$$\text{for } L_{10} \le x_2 \le L_{10} + L_9 \tag{17}$$

$$M = -M_2$$
$$\text{for } 0 \le x_2 \le L_{10} \tag{18}$$

In the above equations, the shear forces, moments, and spring forces are all unknown; however, one spring force can be determined by a vertical force balance:

$$F_1 = P - V_1 - V_2 - F_2 - F_3 - F_4 - F_5 - F_6 - F_7 - F_8 - F_9 \tag{19}$$

where P is a known wheel load (e.g., 157 kN or 35 kips). The strain energy can now be written where k_i is the stiffness of spring i:

$$\begin{aligned} U = &\int_0^{L_1} \frac{M^2}{2EI} dx_1 + \int_{L_1}^{L_1+L_2} \frac{M^2}{2EI} dx_1 + \int_{L_1+L_2}^{L_1+L_2+L_3} \frac{M^2}{2EI} dx_1 + \\ &\int_{L_1+L_2+L_3}^{L_1+L_2+L_3+L_4} \frac{M^2}{2EI} dx_1 + \int_{L_1+L_2+L_3+L_4}^{L_1+L_2+L_3+L_4+L_5} \frac{M^2}{2EI} dx_1 + \int_0^{L_{10}} \frac{M^2}{2EI} dx_2 + \\ &\int_{L_{10}}^{L_{10}+L_9} \frac{M^2}{2EI} dx_2 + \int_{L_{10}+L_9}^{L_{10}+L_9+L_8} \frac{M^2}{2EI} dx_2 + \int_{L_{10}+L_9+L_8}^{L_{10}+L_9+L_8+L_7} \frac{M^2}{2EI} dx_2 + \\ &\int_{L_{10}+L_9+L_8+L_7}^{L_{10}+L_9+L_8+L_7+L_6} \frac{M^2}{2EI} dx_2 + \frac{F_1^2}{2k_1} + \frac{F_2^2}{2k_2} + \frac{F_3^2}{2k_3} \\ &+ \frac{F_4^2}{2k_4} + \frac{F_5^2}{2k_5} + \frac{F_6^2}{2k_6} + \frac{F_7^2}{2k_7} + \frac{F_8^2}{2k_8} + \frac{F_9^2}{2k_9} \end{aligned} \tag{20}$$

Castigliano's theorem is used to create the number of equations needed to solve for the unknown spring forces and boundary conditions (moment and shear force). In this case, 12 unknown variables exist (8 spring forces, 2 reaction moments, and 2 reaction forces). From Castigliano's theorem:

$$\begin{aligned} &\frac{\partial U}{\partial F_2} = \frac{\partial U}{\partial F_3} = \frac{\partial U}{\partial F_4} = \frac{\partial U}{\partial F_5} = \frac{\partial U}{\partial F_6} = \frac{\partial U}{\partial F_7} = \frac{\partial U}{\partial F_8} = \frac{\partial U}{\partial F_9} = 0, \\ &\frac{\partial U}{\partial M_A} = \frac{\partial U}{\partial M_B} = 0, \quad \text{and} \quad \frac{\partial U}{\partial V_A} = \frac{\partial U}{\partial V_B} = 0 \end{aligned} \tag{21}$$

With these relationships a set of 12 equations and 12 unknowns is developed by substituting the moment expressions (9-23) into (24). These expressions can be written in matrix form:

$$\mathbf{MF} = \mathbf{P} \tag{22}$$

where:

P is the load vector.
M is a 12 x 12 matrix of coefficients of the external forces.
F is a column vector of the external forces $F_2 - F_9$, M_A, V_A, M_B, and V_B .

The solution to this matrix equation gives the forces in each of the springs. The spring deflections are:

$$d_i = \frac{F_i}{k_i} \tag{23}$$

where:

d_i is the deflection of spring i.
F_i is the force in spring i.
k_i is the stiffness of spring i.

1.3.3 Comparison of Winkler and Discrete Models

The two models are now compared. Experimental results have shown the Winkler Model is a good representation of track deflection (Zarembski and Choros, 1980; Norman, 2004). Therefore, the discrete model should give results similar to the Winkler Model for similar inputs. The discrete model will, however, have the additional ability to represent non-uniform track.

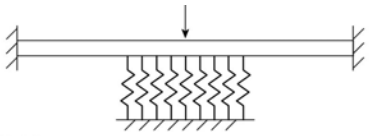

(A) Model

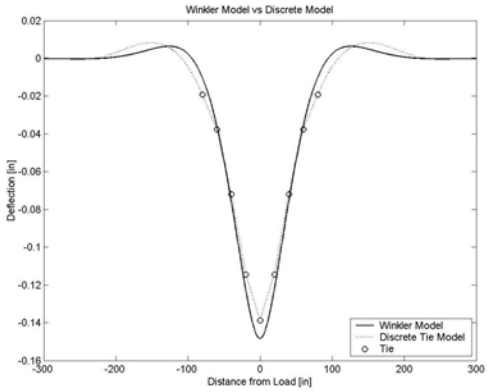

(B) Uniform Track Structure

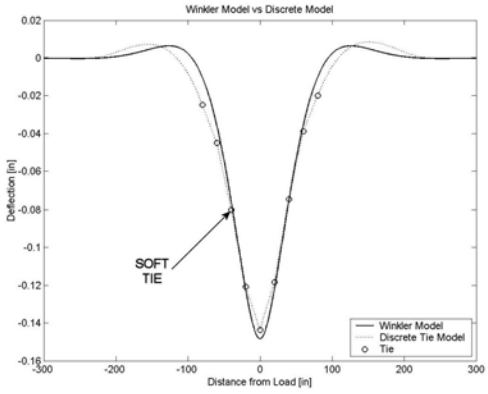

(C) Added Soft Tie

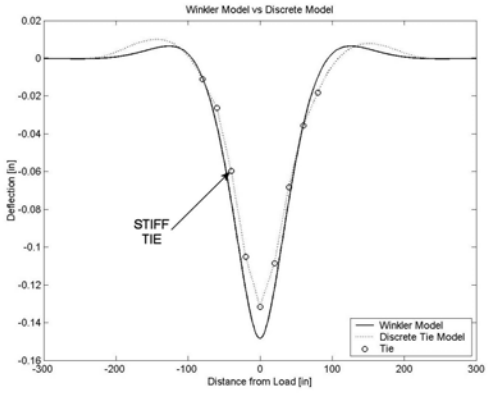

(D) Added Stiff Tie

Figure 5. Comparison of Winkler and Discrete Models

Figure 5(B) compares the deflections from the two models for uniform modulus. The continuous line represents the Winkler Model, and the boxes indicate the tie locations in the discrete model. The track modulus used in the Winkler Model was 20.7 MPa (3000 lbf/in./in.), and the corresponding tie stiffness was 10.5 MN/m (60000 lbf/in.). Track modulus is equated to tie stiffness by dividing by the tie spacing (ties spacing of 50.8 cm (20")). A single point load of 157 kN (35750 lbf) (representing a single vehicle wheel) was applied over the center tie. The deflection predicted by both models is very similar with a maximum error of 6.47 percent (assuming the accepted Winkler Model is correct).

Real track has non-uniform modulus, and these differences can be represented by the discrete model. In Figure 5(C), the stiffness of the third tie from the left end has been decreased by 50 percent (to 5.25 MN/m or 30000 lbf/in.). In Figure 5(D), the stiffness of the third tie has been increased by 100 percent (to 21.0 MN/m or 120000 lbf/in.). In both cases the Winkler Model is shown with a uniform modulus.

The track deflection with a single soft tie (Figure 5(C)) is no longer symmetric about the loading point. The rail is deflected more on the left side of the load where the soft tie is located. The maximum deflection of the rail was also slightly increased (by approximately 0.1219 mm (0.0048 in.)). Figure 5(D) shows the rail deflection where the stiffness of the third tie has been doubled to 21.0 MN/m (120000 lbf/in.). The discrete model shows that the deflection near the stiff tie and the maximum deflection have both decreased (by approximately 0.1829 mm (0.0072 in.)). The results from these examples show that the two models give similar results for similar inputs and the deflection curve can be affected by a single tie.

1.4 Modeling and Simulation

1.4.1 Dynamic Railcar Model

A planar railcar model was used for each rail, and this model is used to predict the performance of the sensor system presented in this research. This prediction is then compared to the results of the experimental field measurements presented in Section 6. The model allows for horizontal (x) and vertical (y) motion, as well as planar rotation of the car body and both trucks. In Figure 6, the car body and both trucks each have an associated mass, and the car body is separated from each truck by a spring/damper suspension system. The model represents dynamic interaction between the railcar and the track model presented in the previous section through the wheel contact loads (P_1 - P_4). Changes in track modulus or changes in track geometry will cause changes in dynamic loading at each wheel.

The equations of motion can now be written for the car body:

$$F_A + F_B - M_{car} g = M_{car} \ddot{y}_{car} \tag{28}$$

$$F_A L - F_B L = I_{car} \ddot{\theta}_{car} \tag{29}$$

and for each truck (assuming small angles):

$$P_1 + P_2 - F_A - M_A g = M_A \ddot{y}_A \tag{30}$$

$$P_1 l - P_2 l = I_A \ddot{\theta}_A \tag{31}$$

$$P_3 + P_4 - F_B - M_B g = M_B \ddot{y}_B \tag{32}$$

$$P_3 l - P_4 l = I_B \ddot{\theta}_B \tag{33}$$

In the above equations, L is the distance between the car body center and truck center. The distance between each wheel and the truck center is l.

Expressions for the forces F_A and F_B can be determined from the free body diagrams for the suspension system (spring and dampers):

$$F_A = k_A\left(y_A - y_{car} - L\sin\theta_{car}\right) + b_A\left(\dot{y}_A - \dot{y}_{car} - L\sin\theta_{car}\right) \tag{34}$$

$$F_B = k_B\left(y_B - y_{car} + L\sin\theta_{car}\right) + b_B\left(\dot{y}_B - \dot{y}_{car} + L\sin\theta_{car}\right) \tag{35}$$

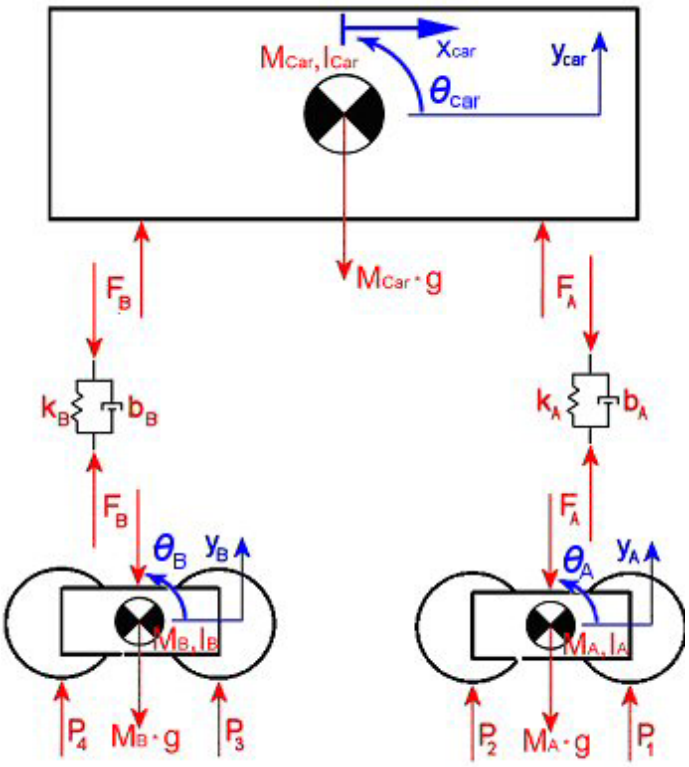

Figure 6. Railcar Free Body Diagrams

The horizontal motion is considered an input derived from the train velocity, and it is assumed that each wheel maintains rail contact. The angle of each truck, therefore, is related to the displacement of its wheels. For Truck A, the relationship is:

$$y_A = \frac{y_1 + y_2}{2} \tag{36}$$

$$\sin\theta_A = \frac{y_1 - y_2}{2l} \tag{37}$$

where each y_i corresponds to the displacement at the wheel contact points (e.g., y_1 corresponds to the displacements at load P_1) and l is the length of the truck. The deflection of the wheels can then be shown to be:

$$y_1 = y_A + l\theta_A \tag{38}$$

$$y_2 = y_A - l\theta_A \tag{39}$$

Wheel displacements are now expressed in terms of truck displacements and angles.

Since the trucks are far apart and the rotation of the car body is small, it is assumed no interaction exists between the wheel loads at Truck A and Truck B (however, interaction can occur from the left to the right rail for a given truck). Therefore, if the Winkler Model (Equation 7) is used and the deflections are superposed, the deflection at wheels 1 and 2 of Truck A are:

$$y_1 = \frac{P_1\beta_1}{2u_1} + \frac{P_2\beta_2}{2u_2}\alpha_2 \tag{40}$$

$$y_2 = \frac{P_2\beta_2}{2u_2} + \frac{P_1\beta_1}{2u_1}\alpha_1 \tag{41}$$

where:

$$\alpha_1 = e^{-\beta_1 x}\left(\cos\beta_1 x + \sin\beta_1 x\right) \tag{42}$$

$$\alpha_2 = e^{-\beta_2 x}\left(\cos\beta_2 x + \sin\beta_2 x\right) \tag{43}$$

Equations 40 and 41 determine the deflections at each of the applied loads, P_1 and P_2. These equations are the result of using the Winkler Model (Equation 7) and superposition of both loads.

Finally, the wheel contact forces ($P_1 \ldots P_4$) are determined assuming a quasistatic interaction with the rail:

$$P_1 = \frac{2u_1}{\beta_1}\frac{y_1 - \alpha_2 y_2}{1 + \alpha_1\alpha_2} \tag{44}$$

$$P_2 = \frac{2u_2}{\beta_2}\frac{y_2 - \alpha_1 y_1}{1 + \alpha_1\alpha_2} \tag{45}$$

1.4.2 Sensor Model

The track and car models above are used with a model of the sensor system to emulate the measurement system. The sensor model is a kinematic relationship between the sensors and rail. The sensor system has two line lasers and a camera. The line lasers intersect the rail surface at an acute angle to create curves across the surface of the rail (Figure 1). The camera then observes the distance between the two laser lines, *d*. A computer uses a mathematical model to calculate the track modulus from this reading.

Figure 7 shows the kinematics of the sensor system. It is assumed that the sensor system is rigid with respect to the wheel contact point (H is constant). This is a reasonable assumption as the instrument beam, truck, and wheels are all massive, nearly rigid elements, and these elements do not include the suspension of the railcar. Rotation of the side frame ($\square_A$) could cause this distance (H) to change, but this rotation has been experimentally shown to be insignificant (Norman, 2004). This value (*H*) is needed for calibration of the system, and this can be accomplished by taking measurements over a location of known modulus (Norman, 2004).

The sensor system measures the distance between the camera image plane and the rail surface, h. The displacement of the rail surface with respect to the wheel/rail contact plane, y_r ($y_r = H - h$), can then be found. The displacement, y_r, can be related to the absolute rail deflection (with respect to the undeflected/unloaded rail), y_{camera}, and the absolute deflection of the wheel/rail contact point, y_{wheel} ($y_r = y_{camera} - y_{wheel}$).

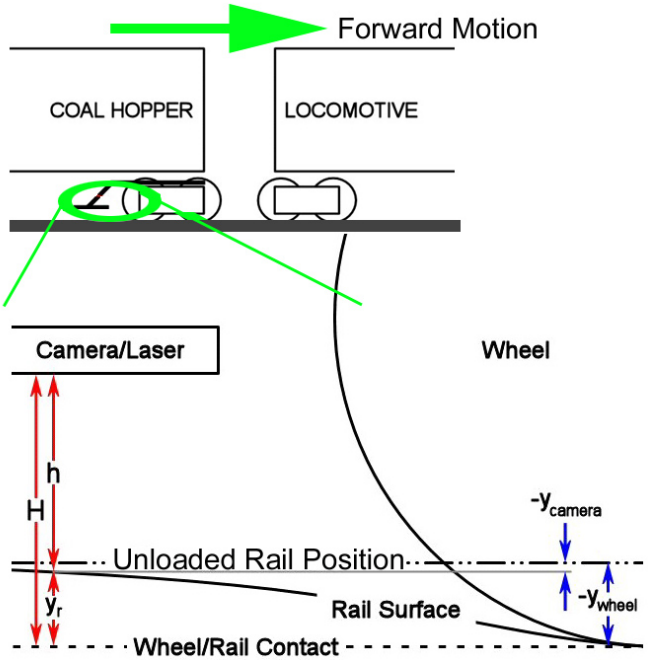

Figure 7. Sensor System Model

Finally, height of the sensor system above the rail surface, h, can be geometrically related to the sensor reading (*d*) giving the distance between the laser curves, Figure 8.

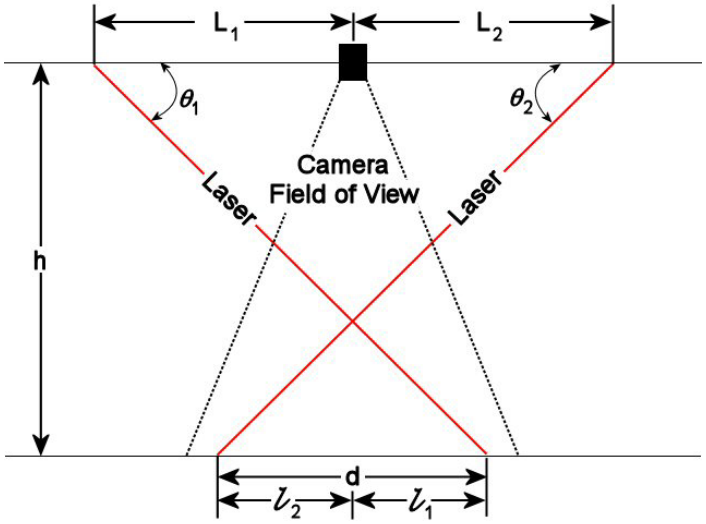

Figure 8. Sensor System Geometry

The height of the sensor system above the rail (h) can be related to the sensor reading (d) with the following geometry:

$$(L_1 + l_1)\tan\theta_1 = h \tag{49}$$

$$(L_2 + l_2)\tan\theta_2 = h \tag{50}$$

$$d = l_1 + l_2 \tag{51}$$

where:

L_1 and L_2 are the horizontal positions of the lasers from the camera.
θ_1 and θ_2 are the angles between the lasers and the horizontal.
l_1 and l_2 are the distances from the camera's centerline and the rail/laser intersection.

Substituting l1 and l2 from (49) and (50) into (51) gives (d):

$$d = \frac{h}{\tan\theta_1} + \frac{h}{\tan\theta_2} - (L_1 + L_2) \tag{52}$$

Combining this information with the track model (e.g., Winkler Model (Equation 7)), the sensor reading (d) can be related to the track modulus (u). The relationship is nonlinear because of the nonlinear track model. Figure 9 shows curves for the system for three different distances between the camera image plane and the wheel/rail contact point (H). Changing this distance shifts the curve and changes the system's sensitivity. Therefore, the sensor system should be mounted at a height (H) that is appropriate for the type of track to be measured. This parameter (H) must be found to calibrate the system using trackside measurements as described in the following section.

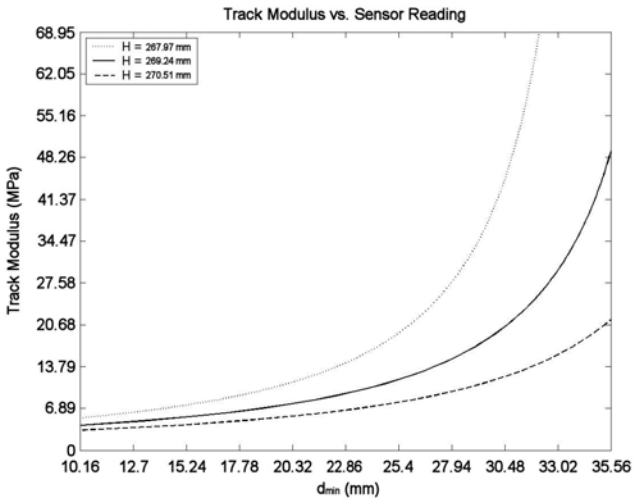

Figure 9. Track Modulus (u) versus Sensor Measurement (d)

1.5 Trackside Measurements

The sensor measurements are first calibrated using independent trackside measurements. Then, other independent trackside measurements are then made to verify the system's performance. True track modulus was determined by making trackside deflection measurements. In Figure 10, rail deflection was measured at a given location using linear variable differential transformers (LVDTs) as a slow moving train passed. The LVDTs were mounted to steel rods driven (about 1 m (3')) into the subgrade to provide a stable reference.

Figure 11 shows a comparison of a typical trackside measurement and a curve fit using the Winkler Model. Again, the rail parameters (I, E) and applied load (car weight) are known; therefore, a track modulus (u) is chosen to fit the trackside measurements. At this example location the track modulus was determined to be 19.3 MPa (2800 lbf/in./in.). The trackside data (solid) match the model (dotted) very well with the exception of some high frequency noise caused by vibration.

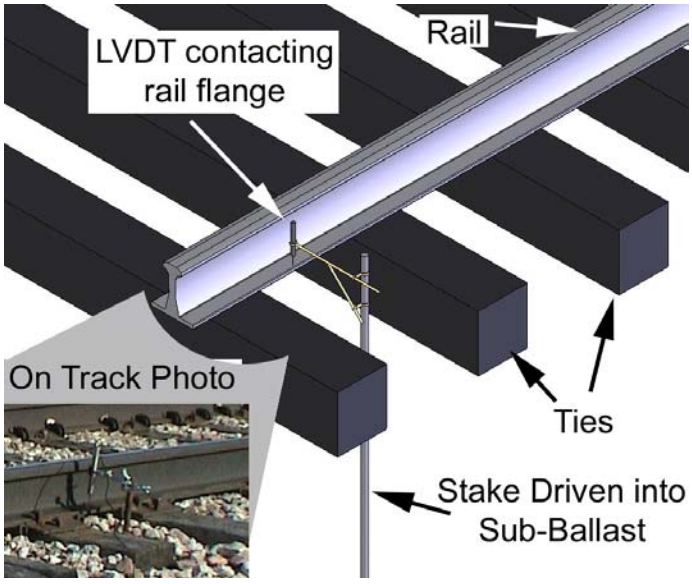

Figure 10. Trackside LVDT Measurements

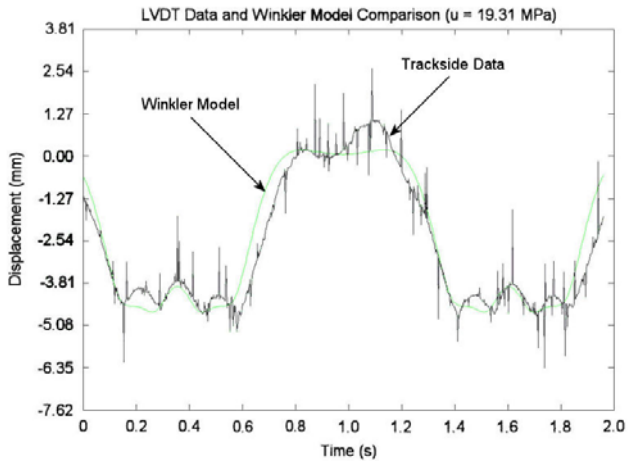

Figure 11. Comparison of Model and Trackside Data

1.6 System Testing

The system has been tested at various locations and for various speeds on Class III and IV tracks. The test setup will be briefly described and testing will be shown for three sections of tangent track. The first two test sites, labeled Site A and Site B, are at slow speeds (~8 km/hr (~5 mph)). Trackside measurements were used to verify the sensor system at these locations, and simulation results are also presented. Finally, at the third site, Site C, the sensor system is tested at various train speeds. Other system testing, not presented in this research, covers over 125 km (70 mi) of Class V track and 42 km (25 mi) of Class IV track (McVey, 2005). The test sites presented in this research were chosen to demonstrate the accuracy of the measurements, show the importance and capabilities of the discrete tie model, and show the consistency of the measurements at different train speeds.

1.6.1 Field Test Arrangement

The sensor system consists of two cars. The first is a heavy vehicle with the sensors attached to the side frame of the truck. The second is a refurbished caboose used to carry human operators and support equipment, such as computers and a power source. The spring displacement on the heavy car's suspension is measured to estimate the load (dynamic and static) at the wheels near the sensor system.

Figure 12 shows typical sensor images. The video images show the line lasers intersecting the top of rail. An odometer is also displayed, showing the location of the measurement along the track (corresponding GPS measurements are recorded but not shown here). The video images are recorded and post-processed. The lasers are first isolated using color filtering and threshold algorithms. The curve of each laser is then fitted with a second order polynomial. Finally, the minimum distance between these two polynomials is found analytically. Curve fitting a polynomial makes the system robust to small variations in rail head profile (Norman, 2004).

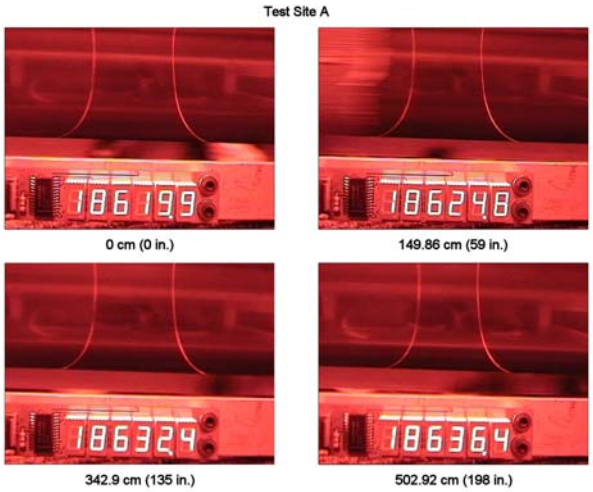

Figure 12. Typical Test Images

1.6.2 Test Site A–System Verification

The first test presented is for a 10m (33') section of tangent (straight) track. The sensor readings are compared to trackside measurements and the dynamic simulation.

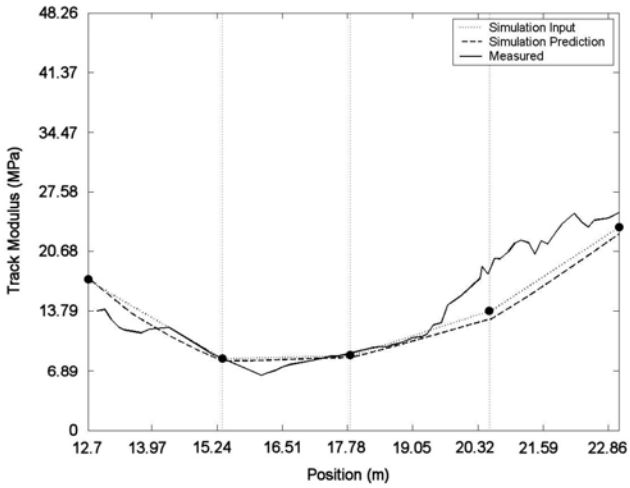

Figure 13. Site A: Trackside, Simulation, and Field

Figure 13 shows the results where the black dots represent trackside measurements of modulus. Linear interpolation was used to estimate the track modulus between these five discrete measurements (straight solid line). This estimate of track modulus was used as the input to the track model used in the simulation. The sensor system's performance was then simulated using the train car dynamics (Equations 44 and 45) and sensor mathematics (Equation 52) described above. The simulated modulus measurements are shown as a dashed line. The final curve (solid) represents the real measurements made by the sensor system.

The simulation (dashed) gave very similar results to the trackside measurements. It is expected that the simulation results are similar to the trackside measurements because the trackside measurements were used as the input. However, small discrepancies occur because of dynamic effects and angular motion of the side frame.

The measurements made by the sensor system also match the trackside measurements very well. The maximum discrepancy between the trackside modulus measurement and the on board sensor measurements occur at 22.3 m with a maximum error of ~5 MPa (709 lbf/in./in.). This error is well within an acceptable tolerance for the sensor system.

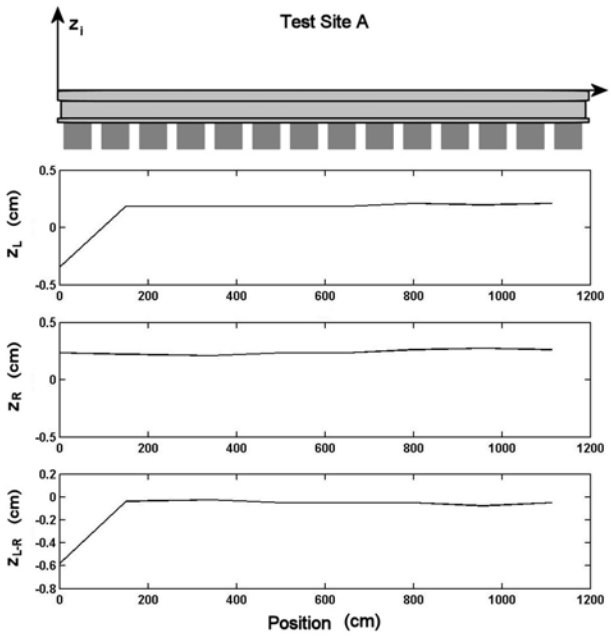

Figure 14. Track Geometry at Test Site A

Figure 14 shows the track geometry measurements for Test Site A. The absolute height of the rail was measured for both rails using a surveyor's transit. The figure also shows cross-level measurements (height of one rail with respect to the other). Such variations in track geometry have been a limitation to previous systems (Carr, 1999). These results show this sensor system, based on relative measurements, is robust to such variations. Extreme variations in track geometry will cause errors in modulus measurement if the errors occur over short distances (~1m). Such dramatic geometry changes are, however, not acceptable for commercial rail and are detectable with other commonly used track geometry systems (Norman, 2004).

1.6.3 Test Site B–Usefulness of The Discrete Model

Test Site B is a section of tangent Class III track. In Figure 15, the sensor measurements (dark solid line) are compared with track side measurements (boxes) and simulation. This test section is interesting because the real sensor measurements matched the trackside measurements well at each of these discrete locations (12.7, 14.22, 16.26, and 17.78 m referenced from the nearest milepost). The agreement between the sensor readings and the trackside measurements validates the sensor system.

If it is assumed that the track modulus varies linearly between these discrete measurements, however, large disagreement exists between the sensor readings and this linearly interpolated estimate of modulus. The discrete tie model, where each tie can take on a different stiffness value, is needed to estimate track modulus at these intermediate locations. Using this model allows variable tie stiffness to be included in the simulation. Because of the agreement between the sensor readings and the independent discrete trackside measurements it is believed that the variation between the trackside measurements, is real (softer and/or stiffer

ties) and that the discrete tie model is needed to produce a good estimate of modulus between these locations.

The results of the simulation using the discrete tie model and placing the four stiffer ties and two softer ties the simulation results (dashed) matched the sensor system measurements (solid). Allowing individual ties to have different stiffness values led to a simulated estimate that matched both the sensor readings and the trackside measurements.

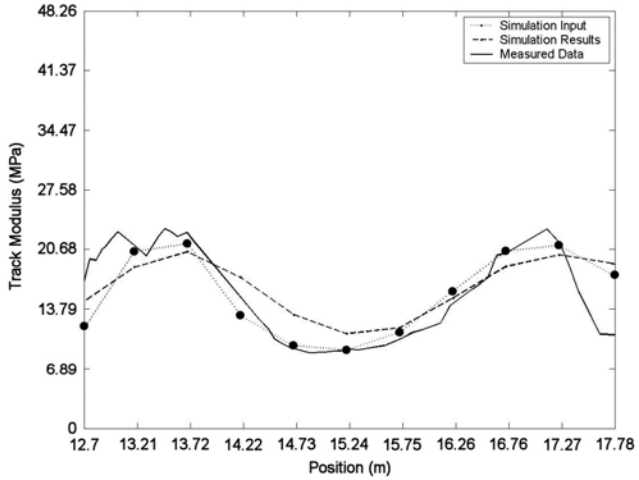

Figure 15. Mile Post 31 East: Trackside Data, Discrete Model Simulation, and Sensor Measurements

Measurements of track geometry were made at Test Site B (similar to Figure 14), and no correlation existed between changes in geometry and changes in track modulus (Norman, 2005). This again suggests that the measurement system can accurately estimate track modulus in the presence of normal variations in track geometry.

1.6.4 Test Site C–Effects of Speed

In Figure 16, Test Site C is a 60 m (200') section of Class IV tangent track where several measurements were repeated at different train speeds 8, 16, 32, 48 and 65 km/hr (5, 10, 20 ,30, 50 mph). It can be seen that modulus measurements are consistent at each of these train speeds with an average standard deviation between the measurements of only 345 lbf/in./in. At higher train speeds where abrupt variations (spikes) exist in track modulus, an overestimate of these variations occurs. This suggests slight error in measurements resulting from dynamic loads.

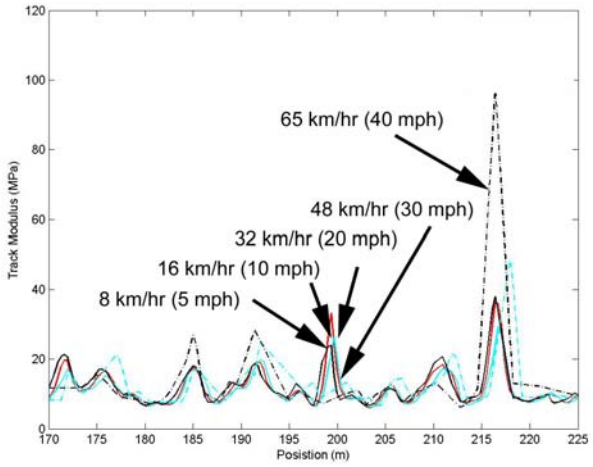

Figure 16. Effects of Speed–Test Site C

Figure 17 shows the averages of several measurements for both rails at Test Site C. These results show good agreement between the rails with two notable exceptions where the right rail is stiffer than the left and where the left is stiffer than the right. These can be generally attributed to neighboring crossties that are not parallel. This causes two ties to be very close on one rail and have wider spacing on the other.

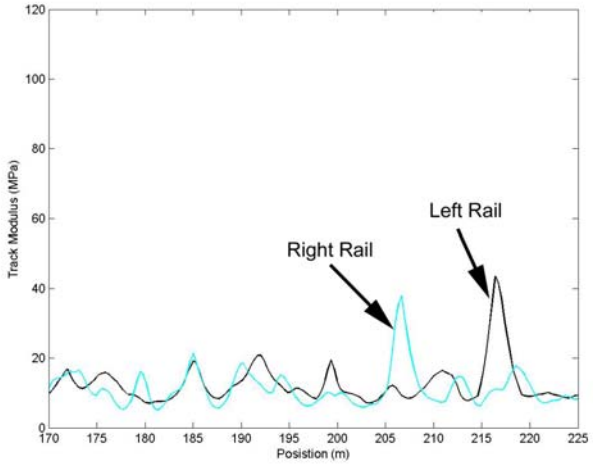

Figure 17. Variation between Rails–Test Site C

2 SUMMARY AND CONCLUSIONS

The modulus of railroad track plays a major role in its ability safely support rail vehicles. This research presented the design, modeling, and testing of a sensor system capable of measuring track modulus over long distances from a moving railcar.

The report presents the Winkler Model and a derivation of a discrete tie model as methods to relate track deflection to track modulus. These models are used to calculate track modulus from the measurements made by the sensor system. The sensor system was modeled to show how the measurements are related to track modulus. In addition, a dynamic model of a railcar is presented, and this model is used to simulate sensor output.

The proposed sensor system was tested at several locations on various types of track. Independent trackside measurements of track modulus and simulations results were used to verify the accuracy of the sensor system. The testing showed that the system was able to measure the correct trend in track modulus (Test Sites A and B). They also suggest the system's ability to correctly resolve modulus changes from tie to tie (Site B). Finally, test results showed the system's ability to consistently measure track modulus at train speeds up to 65 km/hr (40 mph) and to identify modulus variations between both rails (Site C).

3 REFERENCES

[1] Cai, Z., Raymond, G.P., and Bathurst, R.J., 1994, "Estimate of Static Track Modulus Using Elastic Foundation Models," Transportation Research Record 1470, pp. 65-72.

[2] Selig, E.T., and Li, D., 1994, "Track Modulus: Its meaning and Factors Influencing It," Transportation Research Record 1470, pp. 47-54.

[3] Sussmann, T.R., Ebersohn, W., and Selig, E.T., 2001, "Fundamental Nonlinear Track Load-Deflection Behavior for Condition Evaluation," Transportation Research Record 1742, pp. 61-67.

[4] Ebersohn, W., and Selig, E.T., 1994, "Track Modulus on a Heavy Haul Line," Transportation Research Record 1470, pp. 73-83.

[5] Read, D., Chrismer, S., Ebersohn, W., and Selig, E., 1994, "Track Modulus Measurements at the Pueblo Soft Subgrade Site," Transportation Research Record 1470, pp. 55-64.

[6] Thompson, R., and Li, D., 2002, "Automated Vertical Track Strength Testing Using TTCI's Track Loading Vehicle," Technology Digest, February 2002.

[7] Boresi, A.P., and Schmidt, R.J., 2003, *Advanced Mechanics of Materials 6th Edition*. John Wiley & Sons, New York, NY: Chap. 5,10.

[8] Zarembski, A. M., and Palese, J., August 2003, "Transitions Eliminate Impact at Crossings," *Railway Track & Structures*, pp. 28-30.

[9] Davis, D.D., Otter, D., Li, D., and Singh, S., December 2003, "Bridge Approach Performance in Revenue Service," *Railway Track & Structures*, pp. 18-20.

[10] Carr, G.A., 1999, "Dynamic Response of Railroad Track Induced by High Speed Trains and Vertical Stiffness Transitions With Proposed Method of Measurement," Tufts University, September 1999.

[11] Carr, G.A. and Greif, R., 2000, "Vertical Dynamic Response of Railroad Track Induced by High Speed Trains," Proceedings of the ASME/IEEE Joint Conference, pp. 135-151.

[12] Heelis, M.E., Collop, A.C., Chapman, D.N., and Krylov, V., 1999, "Predicting and Measuring Vertical Track Displacements on Soft Subgrades," Railway Engineering.

[13] Zarembski, A.M. and Choros, J., 1980, "On the Measurement and Calculation of Vertical Track Modulus," Proceedings American Railway Engineering Association, Vol. 81, pp. 156-173.

[14] Kerr, A.D., 1983, "A Method for Determining the Track Modulus Using a Locomotive or Car on Multi-Axle Trucks," Proceedings American Railway Engineering Association, Vol. 84, pp. 269-286.

[15] Kerr, A.D., 1976, "On the Stress Analysis of Rails and Ties," Proceedings American Railway Engineering Association, Vol. 78, pp. 19-43.

[16] Kerr, A.D., and Shenton, H.W., 1985, "On the Reduced Area Method for Calculating the Vertical Track Modulus," American Railway Engineering Association Bulletin, Vol. 86, No. 703, pp. 416-429.

[17] Meyer, M.B., 2002, "Measurement of Railroad Track Modulus on a Fast Moving Railcar," University of Nebraska-Lincoln.

[18] Federal Railroad Administration, March 2001, "T-16: FRA's High Speed Research Car," Research Results, RR01-01. http://www.fra.dot.gov/downloads/Research/rr01_01.pdf
[19] Craig, J.J., 1989, *Introduction to Robotics: Mechanics and Control 2nd Edition*, Addison-Wesley Publishing Company, Inc., Reading, MA: pp. 19-60.
[20] Beckwith, T.G., Marangoni, R.D., and Lienhard V.J.H., 1993, *Mechanical Measurements 5th Edition*, Addison-Wesley Publishing Company, Inc. Reading, MA: pp. 464-469.
[21] Chang, C.S., Adegoke, C.W., and Selig, E.T., 1980, "GEOTRACK Model for Railroad Track Performance," Journal of the Geotechnical Engineering Division, Proc. of the American Society of Civil Engineers, Vol. 106, No. GT11, pp 1201-1218.
[22] Raymond, G.P., 1985, "Analysis of Track Support and Determination of Track Modulus," Transportation Research Record 1022, pp. 80-90.
[23] Li, D., and Selig, E.T., 1998, "Method for Railroad Track Foundation Design I: Development," Journal of Geotechnical and Geoenvironmental Engineering, Vol. 68, No. 7-8, pp 457-470.
[24] Li, D., and Selig, E.T., 1994, "Resilient Modulus for Fine-Grained Subgrade Soils," Journal of Geotechnical Engineering, Vol. 120, No. 6, pp. 939-957.
[25] Ebersohn, W., Trevizo, M.C., and Selig, E.T., 1993, "Effect of Low Track Modulus on Track Performance," International Heavy Haul Association, Proceedings of Fifth International Heavy Haul Conference, pp. 379-388.
[26] Stewart, H.E., 1985, "Measurement and Prediction of Vertical Track Modulus," Transportation Research Record 1022, pp. 65-71.
[27] Wanek, M., 2004, "Quality Instruments for Rail-Flaw Detection," Railway Track and Structures, pp. 19-22.
[28] Li, D., Hass, K., and Meddah, A., 2002, "Moving Closer to Performance-Based Track Geometry Inspection," Railway Track and Structures, pp. 15-17.
[29] Li, D., Thompson, R., and Yoshino, D., 2003, "Evaluation of Track-Gauge-Strength Degradation in Revenue Service," Railway Track and Structures, pp. 19-21.
[30] Norman, C.D., 2004, "Measurement of Track Modulus from a Moving Railcar," Masters Thesis, University of Nebraska-Lincoln.
[31] McVey, B., 2005, "Design of a System to Measure Track Modulus from a Moving Railcar," Masters Thesis, University of Nebraska-Lincoln.

ABBREVIATIONS & ACRONYMS

BNSF	Burlington Northern Santa Fe
FRA	Federal Railroad Administration
ft	feet
GPa	gigapascal
GPS	Global Positioning System
hr	hour
in.	inch
km	kilometer
kN	kilonewton
lbf	pounds-force
LVDT	linear variable differential transformers
m	meter
mi	mile
mm	millimeter
MN	meganewton
MPa	megapascal
mph	miles per hour
OPPD	Omaha Public Power District
psi	pounds per square inch
TLV	track loading vehicle
UP	Union Pacific Railroad
UPRR	Union Pacific Railroad
VTM	vertical track modulus